RSC Advances

PAPER

View Article Online
View Journal | View Issue

Cite this: *RSC Adv.*, 2019, **9**, 8184

Highly exfoliated montmorillonite clay reinforced thermoplastic polyurethane elastomer: *in situ* preparation and efficient strengthening†

Jingshui Xu, *[ab] Lihua Cheng,[a] Zhong Zhang,[a] Ling Zhang,[a] Cen Xiong,[a] Weishan Huang,[b] Yashui Xie[b] and Liping Yang*[c]

Received 10th December 2018
Accepted 6th March 2019

DOI: 10.1039/c8ra10121c

rsc.li/rsc-advances

Highly exfoliated montmorillonite (MMT) clay reinforced thermoplastic polyurethane elastomers (TPUs) were prepared by an *in situ* solution polymerization method. By using small amount of 4,4′-methylenediphenyl diisocyanate (MDI) modified pristine clay (MDI-MMT) as fillers, the mechanical properties of TPUs were greatly improved. For example, with the addition of only 1.0 wt% of MDI-MMT, the resultant TPU/MDI-MMT nanocomposites showed approximately 36% increase in initial Young's modulus, 70% increase in tensile strength and 46% increase in ultimate elongation at break as compared with those of neat TPU. Detailed study showed that, owing to the strong covalent bonding between the MMT sheets and TPU matrix, MMT sheets were highly exfoliated during the polymerization process, and the highly exfoliated MMT sheets gave rise to the greatly improved mechanical properties and thermomechanical properties of TPU/MDI-MMT nanocomposites. The present work demonstrates that the *in situ* preparation of TPU/MDI-MMT nanocomposites by using MDI-MMT as fillers is a highly efficient method for reinforcing TPU.

1. Introduction

Montmorillonite (MMT) clay is a popular candidate as a reinforcing nanofiller in polymer nanocomposites, because it presents exceptional properties, such as high surface area, high aspect ratio, lightweight, economic competitiveness, low price, and high stiffness.[1–3] Among the numerous factors that mainly influence the overall properties of polymer/MMT nanocomposites, the dispersion state of the MMT sheets and the interfacial interactions between the MMT clays and polymer matrices are the most crucial ones affecting the mechanical properties of the nanocomposites.[4] For optimal properties, MMT layers should be well-dispersed in polymer matrices to take advantage of their high aspect ratio and high specific surface area, whereas strong interfacial interactions between MMT clays and polymer matrices would facilitate the stress transfer from the matrix to MMT sheets.[5] Since nanoscale MMT sheets have an extremely high surface area to volume ratio, in a nanocomposite system with strong interfacial interactions, a very small amount of MMT clays may have the potential to significantly improve the stiffness of the material.

Thermoplastic polyurethane elastomers (TPUs) are linear, multi-block synthetic copolymers having great industrial importance and consisting of alternating hard (HS) and soft segments (SS) that separate into microphases or domains. They exhibit a unique combination of strength, flexibility and processability due to their phase separated microstructure (shown in Scheme 1).[6,7] These properties result from a molecular structure with rigid HS domains dispersed in the SS matrix. The SS is formed of amorphous domains generally constituted by long chain polyols. And the HS forms domains mainly composed by a rigid diisocyanate and a short chain extender.[8,9] As a result of this unique microstructure, TPUs exhibit very good impact properties at low temperature, excellent chemical resistance and great flexibility over a broad service temperature, which makes them suitable for a wide range of demanding applications such as automobile parts, construction materials, sports equipment, and medical instruments.[10–13] Despite their versatile properties, a major problem with TPUs is that they usually exhibit low initial moduli and stresses at low to intermediate strains, and it is difficult to increase the elastic modulus of TPU while maintaining its high elasticity.

TPU/MMT nanocomposites have received great attention in the past decades due to their significantly improved mechanical, thermal, and gas barrier properties over those of neat

[a]*Technology Research Center for Lingnan Characteristic Fruits & Vegetables Processing and Application Engineering of Guangdong Province, Food Science Innovation Team of Guangdong Higher Education Institutes, Guangdong University of Petrochemical Technology, Maoming, 525000, China. E-mail: xujingshui2011@126.com; Tel: +86 15915276391*

[b]*Guangyou-Mailon New Materials Research Institute, Guangdong Mailon New Materials Co. Ltd., Shantou, 515061, China*

[c]*Guangdong Gulf New Materials Research Institute, Shenzhen, 518000, China. E-mail: liping.Yang@st-gulf.com; Tel: +86 15989778188*

† Electronic supplementary information (ESI) available. See DOI: 10.1039/c8ra10121c

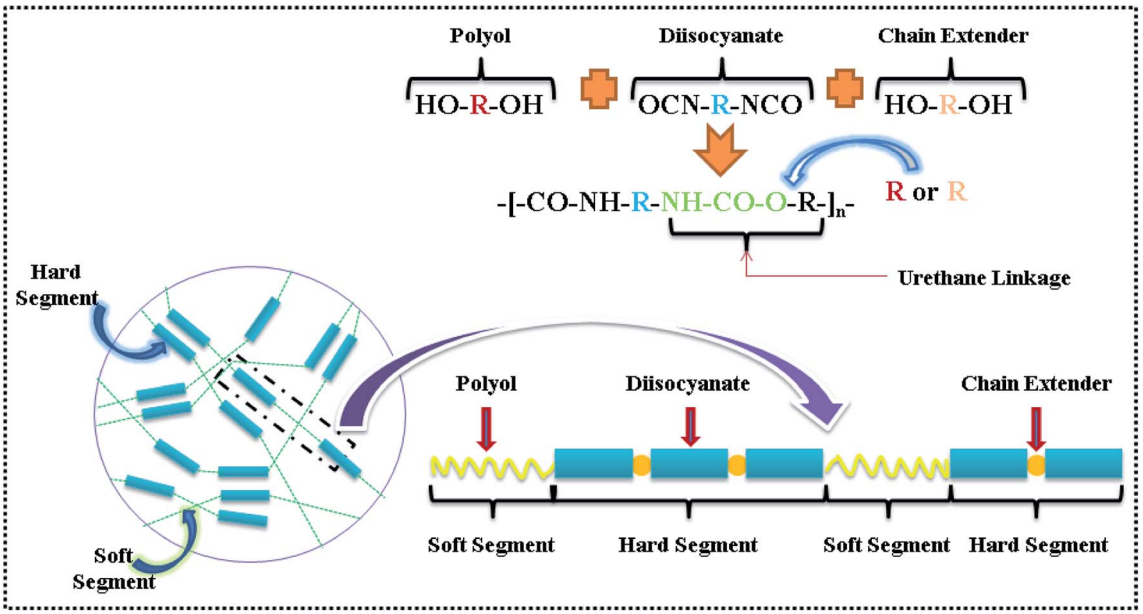

Scheme 1 Schematic of the basic reaction of polyol, diisocyanate and chain extender for synthesis of TPU, morphology of TPU containing hard and soft segments has been represented by different colors.[13]

TPUs.[14–20] Numerous literatures on TPU nanocomposites pay great attention on the effect of methods of preparation, structure of polyurethane, microphase morphology, rheology, mechanical properties, thermal stability, *etc.*[21–32] Wang *et al.*[33] first reported the preparation of the polyurethane (PU)/clay nanocomposites, and concluded that large enhancements in tensile strength and modulus were possible even with intercalated clay particles. To take full advantage of these nanoscale MMT sheets, the key is to exfoliate and disperse the individual MMT layers within polymer matrices, which requires favorable organically modified MMT particles (OMMTs) interactions according to the thermodynamic theory. An appropriate interaction among polymer matrices, MMT clay, and the organic compounds used in modifying the MMT clay is essential to obtain high levels of exfoliation structures.[34–36] The most established method to improve MMT clay dispersion in polymers is to modify the MMT surface, which is required to favor the interfacial interaction. To address this issue, the hydrophilic pristine clays are generally modified by ion exchange, intercalation and grafting reactions.[37]

Traditionally, organic surfactants with long alkyl chains are used to modify MMT surfaces to improve the affinity of polymer matrices with MMT layers and facilitate its exfoliation.[38–41] For example, Qiao *et al.*[42] reported the preparation of the TPU/MMT nanocomposites *via in situ* polymerization, the cetyltrimethyl ammonium bromide (CTAB) was used as a swelling agent intercalated into the galleries of the MMT layers to get the organic MMT; then 4,4′-methylenediphenyl diisocyanate (MDI) was grafted on OMMTs by the reaction with hydroxyl groups on OMMT layers; the obtained results showed that the tensile strength of the nanocomposites showed about 24% increase as incorporating 4.0 wt% of MMT into TPU matrix. Ding *et al.*[43] investigated the TPU/MMT nanocomposites by applying CTAB and MDI as co-treatments for MMT. By incorporating 5.0 wt% MMT, the Young's modulus of the TPU/MMT nanocomposite was 0.61 times lower than that of the neat TPU.

However, the main interfacial interactions between the long alkyl chains and TPU matrix are van der Waals interactions, which are weak interactions inferior in stress transfer as compared with covalent or hydrogen bonds. Furthermore, the long alkyl groups are non-polar that is incompatible with polar polymer systems, resulting in poor dispersion and exfoliation. Importantly, the existence of non-polar long alkyl groups in OMMTs might lead to a lower MDI grafting rate, and the attached MDI on OMMTs was embedded in the long alkyl chains in the subsequent polymerization reaction, which would cause a minor opportunity for reacting with functional groups in TPU chains and thus brought composites a less efficient strengthening effect.

Some of the previous studies have shown that reinforcing nanofillers modified by MDI, *i.e.*, graphene oxide (GO), carbon fiber (CF), carbon nanotube (CNT), *etc.* could improve not only the dispersion of nanofillers in TPU matrix but also the mechanical properties of the resultant TPU nanocomposites.[44,46,47] Worth mentioning that, a feasible strategy to enhance the interfacial interactions in TPU nanocomposites is to prepare the nanocomposites by *in situ* polymerization in the presence of MDI modified MMT clays. It is believed that –NCO groups of MDI could react with hydroxyl (–OH) edge of MMT clay layers while the other –NCO groups afforded the possibility for the reaction with the TPU matrix.[48]

In this paper, the MDI-MMTs were synthesized in *N*,*N*′-dimethylformamide (DMF), which is a polar solvent compatible with TPU reaction system and can guarantee good dispersion and the reactivity of MDI-MMT. There is no non-polar long alkyl group on MMT clay surfaces, thus we hypothesize that MDI

functional groups can play a full role in reacting with TPU system, and bring us an efficient strengthening method. The result shows that the incorporation of MMT sheets into TPU matrix leaded to significant improvements in mechanical properties at very low MDI-MMT loadings. What we focus is to obtain a better understanding and insight into the underlying mechanisms for reinforcement effects observed, which allows us to reveal the pivotal role played by the covalent bonding between MMT sheets and the polyurethane chains in strengthening TPU.

2. Experimental section

2.1. Materials

Pristine sodium montmorillonite [Na-MMT, moisture content (<10 wt%), SiO_2 (48.0–51.0 wt%), Al_2O_3 (13.0–16.0 wt%), MgO (3.721 wt%), CaO (3.712 wt%), Fe_2O_3 (1.858 wt%), K_2O (0.748 wt%)] with cationic exchange capacity of 100 mmol/100 g was obtained from Huai An Saibei Technology Co. Ltd (China).[39] 4,4′-Methylenediphenyl diisocyanate (MDI, 99.8% purity, 33.5 wt% the content of NCO group in MDI, molecular weight 250.25 g mol^{-1}) was purchased from Shanghai Spectra Biotechnology Co. Ltd (China). Polytetramethylene glycol (PTMG, OH value 115.0 mg KOH g^{-1}, water content ~0.0089 wt%, average molecular weight ~1000 g mol^{-1}) and 1,4-butanediol (1,4-BD, molecular weight 90.12 g mol^{-1}) were purchased from Aladdin Chemistry Co. Ltd (China), before use, trace moisture was removed by vacuum at 120 °C. *N*,*N*′-Dimethylformamide (DMF) was purchased from Guoyao Chemical Reagent Co. Ltd (China), before use, DMF was distilled under vacuum. Other reagents (AR) were purchased from Xilong Chemical Co. Ltd (China).

2.2. Preparation of MDI-MMT

The preparation of MDI-modified pristine clay (MDI-MMT) was performed according to the procedure reported by Sadasivuni *et al.*[48] with a minor modification. A calculated amount of Na-MMT was dispersed in dried DMF in a 500 mL, three-necked flask equipped with a stirrer and a thermometer. Excess MDI was added dropwise to the Na-MMT dispersion at 80 °C with continuous stirring. Stop adding MDI until no bubbles were emitted from the reaction system. After the reaction, the MDI-MMTs were obtained as slurry like mixture flocculated in DMF. Then MDI-MMTs were carefully stored for further use after pouring out the upper DMF layer.

2.3. *In situ* synthesis of neat TPU

Neat TPUs were synthesized by an *in situ* solution polymerization method. The ratio *r*, called isocyanate index, (r = [NCO]/[OH]) was approximately 1.02 in all cases, while the ratio of OH groups belong to macrodiol and the chain extender (1,4-BD) was kept constant (R = 1). The dried DMF was employed as reaction medium. The concentration of all reactants in reaction mixture was about 20 wt%. A three necks round-bottomed flask equipped with a water-cooled condenser under N_2 atmosphere at continuous stirring was charged with 5.0 mmol of PTMG, 10.22 mmol of MDI and 25.0 mL dried DMF. The reaction medium was heated up to 65 °C in an oil bath. The reaction was continued for 4.0 h to prepare the NCO-terminated prepolymer, until the theoretical NCO content was attained (~5.8 wt%); and the content of NCO during reaction was determined using the dibutylamine back titration.[45] In the next step, 5.0 mmol of the chain extender (1,4-BD) dissolved in 5.0 mL dried DMF was added using a syringe. The reaction temperature was increased slowly to 80 °C and maintained for another 4.5 h. The reaction mass became highly viscous, which indicated the formation of neat TPU. After degassing in order to remove residual bubbles, then the composite solution was casted in a polytetrafluoroethylene mold and dried at 50 °C for 2.0 days. The residual DMF was removed by placing the film at 80 °C vacuum oven for another 2.0 days. The obtained samples were kept in desiccator before characterization.

2.4. *In situ* synthesis of TPU/MDI-MMT nanocomposites

An *in situ* solution polymerization of TPU/MDI-MMT nanocomposites was performed according to a previous report by Bera *et al.*[44] with slight modification. The ratio *r*, called isocyanate index, (r = [NCO]/[OH]) was approximately 1.02 in all cases, while the ratio of OH groups belong to macrodiol and the chain extender (1,4-BD) was kept constant (R = 1). Briefly, PTMG (5.0 mmol) and dried DMF (10.0 mL) were taken in 250 mL three necks round-bottomed flask equipped with a water-cooled condenser under N_2 atmosphere at continuous stirring. The reaction medium was heated up to 65 °C in an oil bath. A stoichiometric excess of MDI (10.22 mmol) was dissolved in 15 mL of dried DMF and was injected into the reaction medium using a syringe. The reaction was continued for 4.0 h to prepare the NCO-terminated prepolymer, until the theoretical NCO content was attained (~5.8 wt%); and the content of NCO during reaction was determined using the dibutylamine back titration.[45] The required amount of MDI-MMT dispersion in dried DMF was added to the NCO-terminated polyurethane prepolymer. In the next step, 1,4-BD (5.0 mmol) dissolved in 5.0 mL dried DMF was added using a syringe. The reaction temperature was increased slowly to 80 °C and maintained for another 4.5 h. The reaction mass became highly viscous, which indicated the formation of TPU/MDI-MMT nanocomposites. After the solid content of the resultant material was condensed to 20 wt% in DMF, degassing in order to remove residual bubbles, and then the composite solution was casted in a polytetrafluoroethylene mold and dried at 50 °C for 2.0 days. The residual DMF was removed by placing the film at 80 °C vacuum oven for another 2.0 days. The obtained TPU/MDI-MMT nanocomposites were kept in desiccator before characterization. The process for the fabrication of TPU/MDI-MMT nanocomposites is illustrated in Scheme 2.

2.5. Characterization

The FTIR spectra of samples were obtained using a Nicolet 380 spectrophotometer (American Digilab). The samples were applied on dry KBr pellets that are manually prepared using

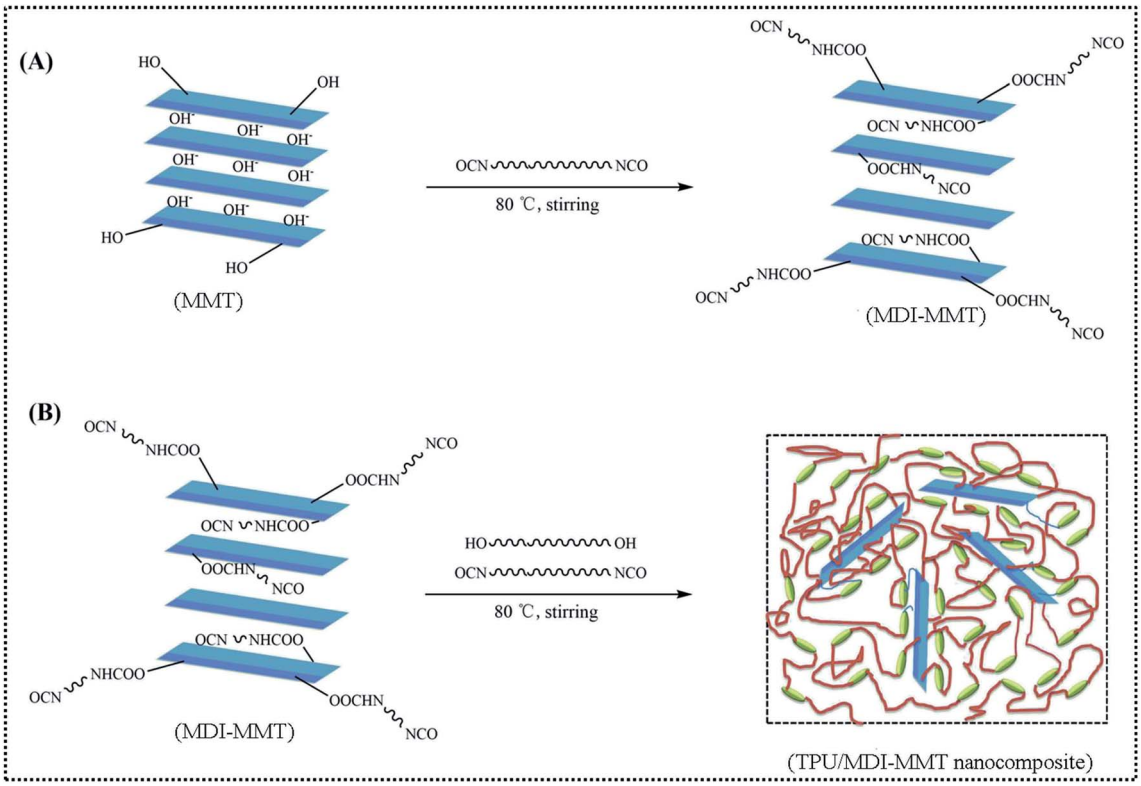

Scheme 2 A schematic representation of the fabrication process of the *in situ* polymerized TPU/MDI-MMT nanocomposites.

a hydraulic press (PerkinElmer, Spain). FTIR spectra were obtained at wave numbers ranging from 4000 cm^{-1} to 400 cm^{-1}.

X-ray diffraction (XRD) analysis was performed on Bruker D8 Advance X-ray diffractometer (STADI P, Germany) with a Cu target (λ = 0.1540 nm) at room temperature. The system consists of a rotating anode generator operated at 40 kV and 40 mA current. The scanned diffraction angle 2θ was scanned from 1.3° to 10° at a scanning rate of 1° per minute and a step distance of 0.02°. Bragg's law was applied to calculate the distance between the silicate layers.

$$2d \sin \theta = n\lambda \quad (1)$$

where, λ is the wavelength of the X-ray, d is the diffraction interplanar distance (nm), and 2θ is diffraction angle (°).

The nanoparticle dispersion within the polymer matrix and the nanocomposite structure was observed by a transmission electron microscope (TEM, JEM-2100, Japan) operating at an accelerating voltage of 200 kV.

The morphology of samples was observed using a SEM (FET Quanta 200F, USA). The samples were mounted on a sample holder by using silver paste and then coated with a thin layer of gold to prevent charging. Incident electron-beam energies from 1.0 keV to 30 keV were used. In all cases, the beam was at a normal incidence to the surface of the samples, and the measurement time was 100 s.

The weight losses of samples were determined using thermo gravimetric analyzer (TGA, NETZSCH STA409PC, Germany). The samples were heated from 20 °C to 800 °C at a heating rate of 10 °C min^{-1} under a nitrogen atmosphere.

The thermal properties of samples were evaluated by means of a differential scanning calorimetry (DSC) Q 200 (TA Instruments) at a heating/cooling rate of 10 °C min^{-1} between −70 °C and 240 °C under nitrogen atmosphere. In order to homogenize the thermal history of the samples, a heating–cooling–heating cycle was applied and the thermal transitions were analyzed based on the cooling and second heating scans. Samples having a mass between 2.5 mg and 6 mg were used. All tests were repeated twice under the same conditions.

The tensile properties of the sample films were investigated by a universal testing machine (Instron 4465, MTS Company, USA) operated at a strain speed of 50 mm min^{-1} with a load cell of 5 kN at room temperature. Tests were conducted according to ISO 178-2011 standard. The data was analysed using the TW4 work test software. At least 5 dumbbell-shaped specimens of the same materials were measured.

Dynamic mechanical analysis (DMA) experiments were measured using a Dynamical Mechanical Analyser (Q800, TA Instruments). Rectangular specimens measuring 8 mm in width and 0.9 mm in thickness were cooled with N_2 gas to −70 °C and subjected to a temperature sweep from −70 °C to 120 °C at a heating rate of 3 °C min^{-1}. The measurements were conducted in tensile mode with frequency of 1 Hz and strain of 0.03%. The storage modulus (E') and loss tangent (tan δ) were recorded. The flow temperature was defined as the onset of inconsistent tan δ data, close to the temperature at which the sample was no longer mechanically robust.

Before rheological testing, samples were vacuum dried at 65 °C for 24 h. The complex viscosities of samples were

measured in an AR 2000 rheometer (TA Instruments) in parallel plate geometry with plates of diameter 25 mm. Only the compressed neat TPU and TPU/MDI-MMT samples were tested using steady shear mode with shear rate ranging from 0.01 to 100 s^{-1} at 200 °C. The oscillation strain was set at 5% to ensure that the dynamic measurements were in the linear viscoelastic range.

3. Results and discussion

3.1. FTIR analysis

The FTIR spectra characterized typical functional groups for different samples. For pristine Na-MMT, transmittance band at 3627 cm^{-1} represents O–H stretching vibration for Al–OH and Si–OH in silicate layers [Fig. 1A(a)]. The band at 1634 cm^{-1} represents a bending vibration in water. Typical bands of silicate at 1035 cm^{-1} is representative of Si–O, while Al–O stretching vibration is in the range of 400 cm^{-1} to 600 cm^{-1}. In Fig. 1A(b) for MDI-MMT, transmittance bands at 1650–1750 cm^{-1} represent C═O stretching vibration. The bands at 3300–3500 cm^{-1} represent N–H stretching vibration, and the bands at 1500–1600 cm^{-1} represent N–H bending vibration.

The appeared peaks in FTIR spectra of neat TPU and its nanocomposites are assigned to their respective functional groups [Fig. 1(B)]. The comparison of the neat TPU and its nanocomposites indicates that all the characteristic peaks of the neat TPU remain unchanged in TPU/MDI-MMT nanocomposites. The absorption peak at 2270 cm^{-1} ascribed to the isocyanate groups (–NCO) in neat TPU and its nancomposites disappeared completely, indicating full NCO conversion and absence of residual –NCO.[18,19] The peak at 3325 cm^{-1} is the characteristic stretching vibration of hydrogen bond [Fig. 1(C)]. In Fig. 1(D), the free and hydrogen bonded carbonyl stretching vibration peaks in neat TPU or the TPU/MDI-MMT nanocomposites appear at 1726 cm^{-1} and 1701 cm^{-1}, respectively, indicating that NH–COO– has been formed. Nevertheless, the peak at 1649 cm^{-1} corresponding to the characteristic C═O stretching peak of –NHCONH– groups appears obviously in the TPU/MDI-MMT nanocomposites while it is of absence in neat TPU. In the TPU/MDI-MMT nanocomposites, this band is observed to increase in intensity with an increasing loading of MDI-MMT. This phenomenon was observed because some polymer chains with –NCO end groups were close to MMT during the synthesis process and they might react with –OH to form urethane bonds. In the TPU/MDI-MMT nanocomposites, the characteristic absorption peak of MMT (1035 cm^{-1} for Si–O telescopic vibration peaks) still appeared in the curve, indicating that the nanocomposites containing MMT sheets.

3.2. Morphology of the composites

3.2.1. XRD analysis. XRD analysis is one of the most effective means that study the dispersion state of MMT in

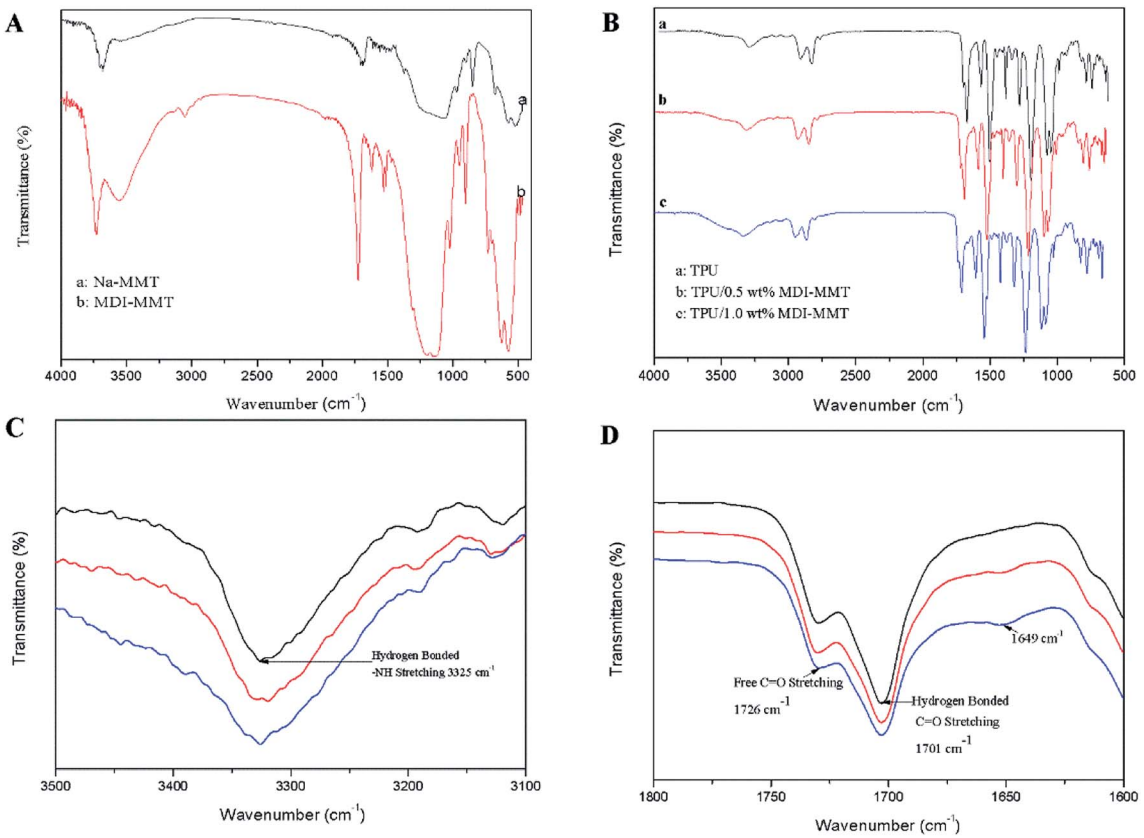

Fig. 1 FTIR spectra of (A) (a) pristine Na-MMT and (b) MDI-MMT; (B) (a) neat TPU and (b and c) TPU/MDI-MMT nanocomposite; (C) free and hydrogen bonded N–H stretching region; and (D) free and hydrogen bonded carbonyl peaks of neat TPU and TPU/MDI-MMT nanocomposites at different MDI-MMT loadings.

polymer matrices. The distribution of MMT layers can be concluded by examining the change on the peak shape and peak position of the characteristic MMT 001 peak. X-ray scattering patterns of the pristine Na-MMT, MDI-MMT, neat TPU and its nanocomposites containing different MDI-MMT loadings are shown in Fig. 2. The reflections of Na-MMT and MDI-MMT appeared at $2\theta = 7.3^\circ$ and $2\theta = 6.8^\circ$, respectively. The interlayer spaces of the pristine Na-MMT and MDI-MMT from the Bragg's equation are 1.2 nm and 1.3 nm, respectively [Fig. 2(a and b)]. The interspace of the Na-MMT clay was expanded by NCO groups of MDI grafted on Na-MMT clay layers. In Fig. 2(c), the TPU has no reflection peaks. As shown in Fig. 3(d–g), no distinct peaks were observed in XRD patterns of the TPU/MDI-MMT nanocomposites. The strong peak at $2\theta = 6.8^\circ$ for the typical interlayer spacing of MDI-MMT has disappeared in the TPU/MDI-MMT nanocomposites, indicating that the MMT layer was completely exfoliated and the MMT sheets were evenly distributed in TPU matrix. Possibly the MDI groups grafted on clay sheets was enrolled in the polymerization process, the formed chemical bonds between clay sheets and polymer matrices made the clay sheets fully exfoliated during the reaction process.

3.2.2. TEM and SEM observations. As the performance of TPU/MDI-MMT nanocomposites strongly depends on the dispersion state of the MDI-MMT fillers in TPU matrix, TEM and SEM were employed to investigate the morphology of the samples. The TEM pictures of the samples are shown in Fig. 3. As shown in Fig. 3(a), we can see that the neat TPU thin slice is transparent and in light color. Dark parts appeared in Fig. 3(a) could be ascribed to the difference on the degree of electron beam penetration for different parts of the sample. Fig. 3(b) showed a typical TEM micrograph of the TPU/MDI-MMT nanocomposites, in which the dark lines marked with arrows represent the intersections of the MMT sheets dispersed in the TPU matrices. From Fig. 3(b), we can see that most of the MMT clays were exfoliated into thin MMT sheets randomly distributed in TPU matrix, while minors MMT clays were still in thin

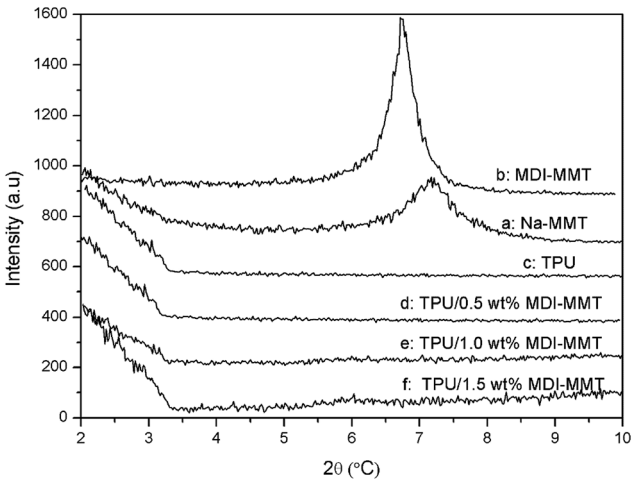

Fig. 2 XRD spectra of (a) pristine Na-MMT, (b) MDI-MMT, (c) neat TPU, and (d–f) TPU/MDI-MMT nanocomposites at different MDI-MMT loadings.

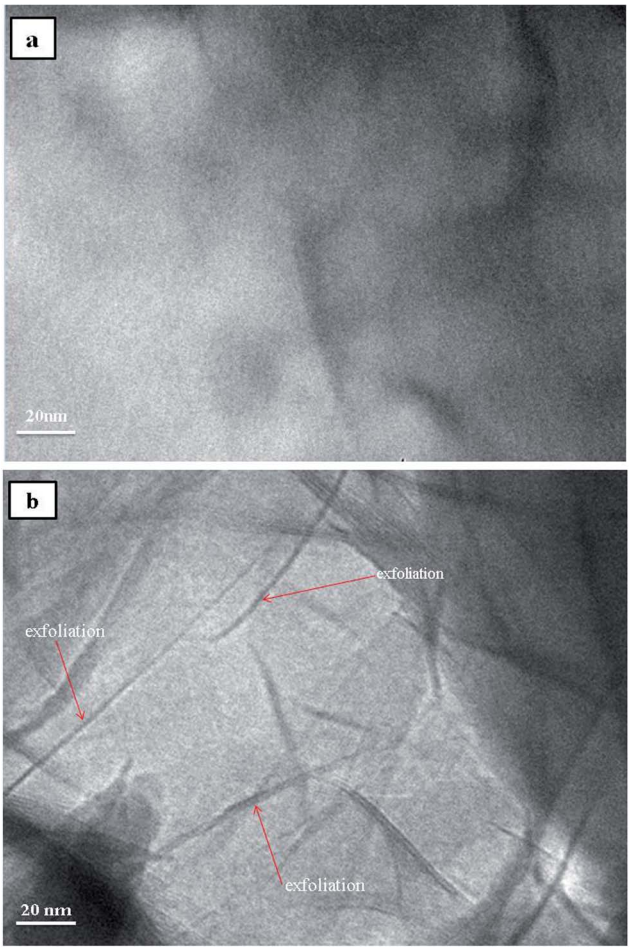

Fig. 3 TEM images of (a) neat TPU, and (b) TPU/MDI-MMT nanocomposites containing 1.0 wt% MDI-MMT.

intercalated stacks.[49] Obviously, the obtained TPU/MDI-MMT nanocomposites showed a majority of exfoliated structure as a whole. This was consistent with XRD results (Fig. 2), which disclosed that MMT clays were well exfoliated in the TPU/MDI-MMT nanocomposites.

In order to get a visualized insight over the dispersion state and interfacial interaction between the MMT platelets and TPU matrix, the tensile fracture surface of TPU/MDI-MMT nanocomposites at different MDI-MMT loadings were investigated by SEM. Results are presented in Fig. 4. SEM image of the tensile fractured surface of neat TPU was relatively smooth [Fig. 4(a)], while the fracture surfaces of the TPU/MDI-MMT nanocomposites were much rough and the roughness increased with the increase of MDI-MMT loadings [Fig. 4(b and c)]. It is affirmed that the exfoliated MMT sheets are almost evenly dispersed in TPU matrix.[16] Furthermore, the surfaces of the TPU/MDI-MMT nanocomposites showed much irregular, even caves, as the loading of 2.0 wt% MDI-MMT [Fig. 4(d)]. Possibly large MMT aggregation took place in TPU matrix, which was reported in the literature.[17] The observed morphology is in consequence with the results obtained from tensile testing which shows better tensile strength at a low MDI-MMT loading below 2.0 wt%.

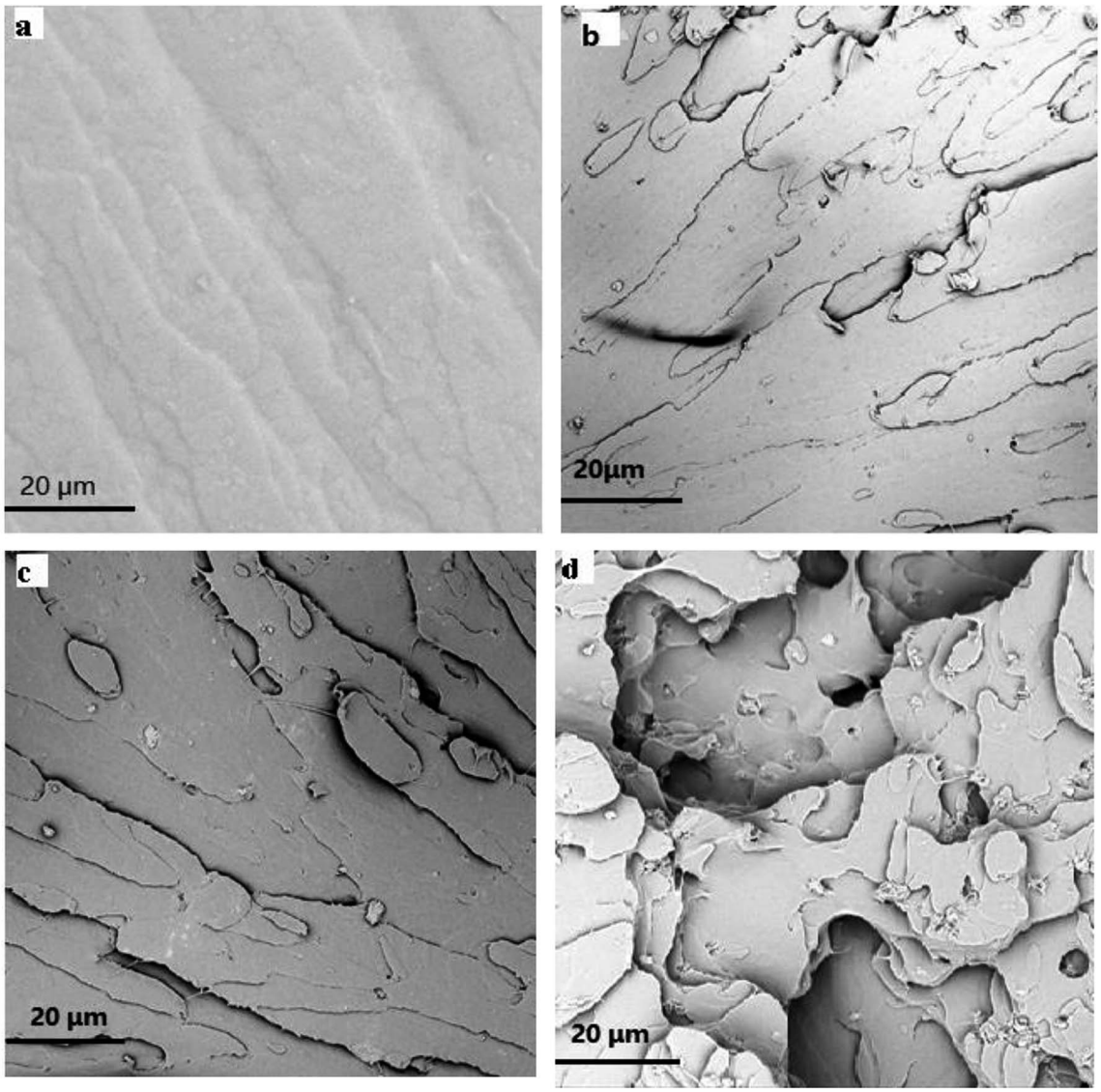

Fig. 4 SEM photomicrographs of the tensile fracture surface on (a) neat TPU, and (b–d) TPU/MDI-MMT nanocomposite at different MDI-MMT loadings (0.5 wt%, 1.0 wt%, 2.0 wt%).

3.3. Thermal behavior of TPU composites

3.3.1. TGA analysis. Thermal properties of the samples are also investigated to fully understand the influence of MMT sheets in TPU. Fig. 5 shows the TGA plots of the samples. Both neat TPU and its nanocomposites clearly showed three-stage degradation. The degradation temperatures are summarized in Table 1. Results indicated that neat TPU began to decompose at a slightly higher temperature as compared with that of the TPU/MDI-MMT nanocomposites [Fig. 5(B)]. However, the TPU/MDI-MMT nanocomposites exhibited a higher resistance at the end of thermal decomposition process. As shown in Fig. 5, when temperatures are below 250 °C, the weight loss of samples is the thermal decomposition of small and unstable oligomer chains [Fig. 5(A)]. In Table 1, T_{10} and T_{50} of TPU are 312 °C and 368 °C, respectively; when the addition amount of MDI-MMT is 0.5 wt%, the corresponding T_{10} and T_{50} of the TPU/MDI-MMT nanocomposites rise to 313 °C, 373 °C, respectively; it is obvious that the corresponding T_{10} and T_{50} increase as the loading level of MDI-MMT increase. These phenomena demonstrated that MMT layers have very good blocking effects on neat TPU. Char residue value also increased as the increase of the addition amount of MDI-MMT, this is because the well dispersed nanoscale MMT sheets have the higher barrier efficiency on the decomposition of polymer matrices.

3.3.2. DSC analysis. The DSC heating curves of neat TPU and the TPU/MDI-MMT nanocomposite containing 1.0 wt% MDI-MMT are depicted in Fig. 6. As the structure of neat TPU includes hard segment and soft segment, generally two melting temperature are expected. The DSC curve shows two small peaks and these endothermic peaks are associated with the melting temperatures of the soft domains ($T_{m(soft)}$) and the melting temperatures of hard segment domains ($T_{m(hard)}$). As shown in Fig. 6, the $T_{m(soft)}$ of neat TPU and the TPU/MDI-MMT

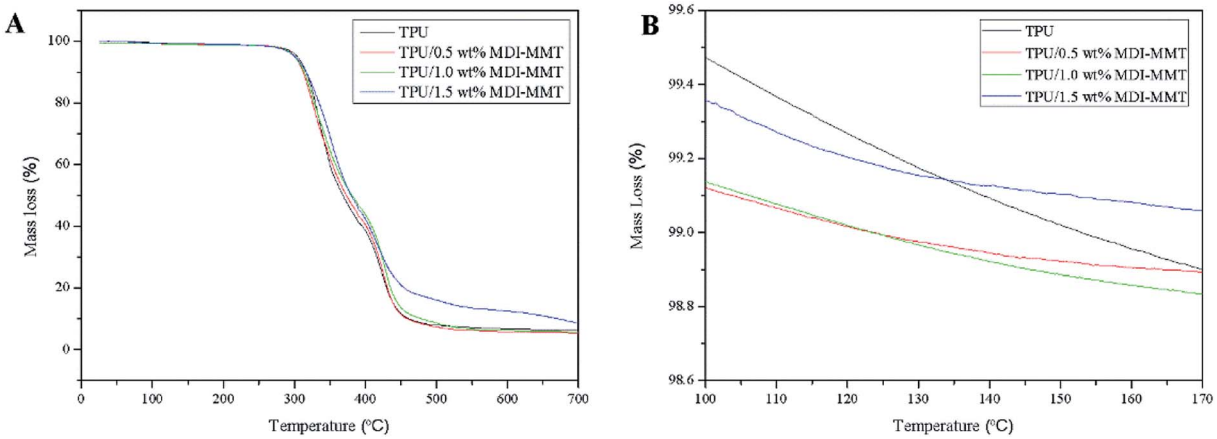

Fig. 5 (A) Representative TGA curves of neat TPU, and TPU/MDI-MMT nanocomposites at different MDI-MMT loadings and (B) TGA curves of neat TPU, and TPU/MDI-MMT nanocomposites from 100 °C to 170 °C.

Table 1 TGA results of neat TPU and TPU/MDI-MMT nanocomposites of 0.5, 1.0 and 1.5 wt% exfoliated MMT layers, respectively

Samples	T_{10} (°C)	T_{50} (°C)	Char residue (%)
Neat TPU	312.1	368.5	3.47
TPU/MDI-MMT (0.5 wt%)	313.3	373.2	4.91
TPU/MDI-MMT (1.0 wt%)	316.1	380.1	5.03
TPU/MDI-MMT (1.5 wt%)	316.5	381.4	5.62

nanocomposites are found to be around 17 °C and 20 °C, respectively. This increase in the $T_{m(soft)}$ could be attributed to the effects produced by the rigid MMT sheets in the soft segment domains, leading to the increase of the degree of crystallinity. This is because the nanoscale MMT sheets affect the crystal structure of the soft segments and tends to increase the melting point of the same with addition of MMT layers due to their nucleation and inhibition effects.[47a] Moreover, the $T_{m(hard)}$ of the neat TPU and its nanocomposites are found to be around 184 °C and 192 °C, respectively. Shifting to $T_{m(hard)}$ of TPU to higher temperature by nucleating effect of nanoscale MMT sheets and restriction of chain mobility of neat TPU.[50] This observation is related with increasing crystallization degree of MMT sheet-filled polyurethane elastomer composites.[25] This phenomenon may be caused from better directionally orientation of TPU chains and enhancement of melt crystallization after importation of the exfoliated MMT layers and TPU matrix.[29]

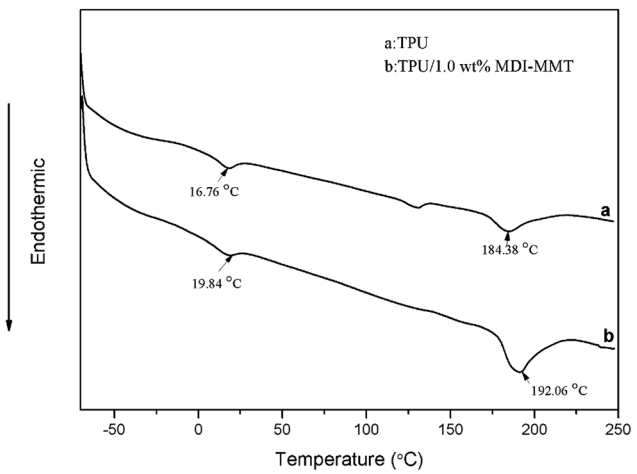

Fig. 6 Typical DSC curves of (a) neat TPU, and (b) TPU/MDI-MMT nanocomposite containing 1.0 wt% MDI-MMT.

3.4. Mechanical properties of TPU nanocomposites

3.4.1. Tensile properties. Typical tensile stress–strain curves of the samples can be divided into three regions, which are presented in Fig. 7. Region I is a quasi-linear region, and the initial modulus measured from this region is governed by the TPU crystallinity and tilting of the hard microdomains in the stretching direction.[51] Further increasing the strain will lead to permanent destruction of the hard micro-domains; the large hard micro-domains will break into smaller ones, and this is followed by two distinct regions of plastic deformation.[5] Herein, we assume 5% strain as the point where the hard microdomains start to break down (that is, the starting point of Region II). In Region II, the slopes of the stress–strain curves initially reduce as the strain increases, owing to the increasing breakdown of the hard microdomains, and then stabilize at a moderate value (Fig. 8), beyond which further plastic deformation in this region is mainly due to the disentanglement of soft microdomains and reorientation of small hard microdomains.[5] Region III starts at roughly 200% strain, which is characterized by a steep upturn in the stress–strain curve that is closely related to the strain-induced crystallization of the soft segments until fracture occurs on reaching the tensile strength.

The tensile properties of the samples are demonstrated in Fig. 8. It is clear that the TPU/MDI-MMT nanocomposites showed better mechanical properties as compared to neat TPU and the tensile properties are dependent on the MDI-MMT loading. It is striking to see that the TPU/MDI-MMT nanocomposite with 1.0 wt% MDI-MMT exhibits higher initial

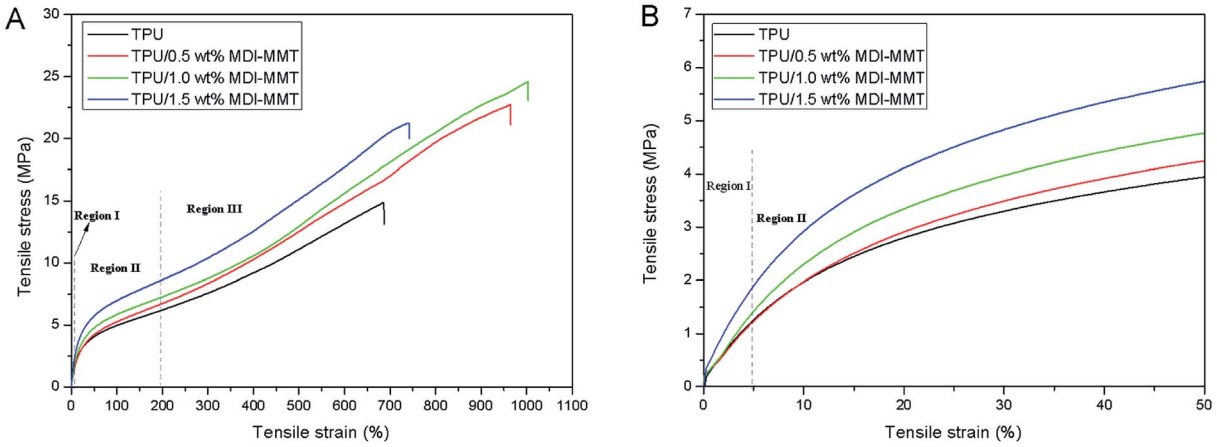

Fig. 7 (A) Representative tensile stress–strain curves of neat TPU and TPU/MDI-MMT nanocomposites at different MDI-MMT loadings; and (B) the stress–strain curves in Regions I and II showing the variation of the initial moduli of neat TPU and TPU/MDI-MMT nanocomposites at different MDI-MMT loadings.

modulus in Region I, higher stress in Region II, and larger ultimate elongation as compared with neat TPU. By incorporating only 1.0 wt% of MDI-MMT into TPU matrix by an *in situ* polymerization, the initial Young's modulus (E^a) of the TPU/MDI-MMT nanocomposite was increased by more than 36%. The prominent increase of the E^a with MMT sheets could be attributed primarily to the effective load transfer offered by the MDI-MMT interface. Possibly the –NCO on the surfaces of MMT sheets were able to form strong covalent bonds with TPU matrix. Furthermore, H-bonding and polar–polar interaction between MMT sheets and TPU chains made the hard domain of TPU stiff and thus increased the tensile modulus of the composites.[52]

From Fig. 7 and 8, it can be concluded that the stress of the TPU/MDI-MMT nanocomposites in Region II is higher than that of the neat TPU and it increases with the increase of the MDI-MMT loadings in TPU/MDI-MMT nanocomposites. The mechanism behind such dramatic improvement of tensile strength could be ascribed to the following factors: (a) strain hardening facilitated by the increasing amount of MMT layers;[53] (b) orientation of TPU grafted MMTs and the soft segment of TPU along the tensile axis improved the tensile strength of the composite greatly.[43] Formation of the covalent bonding between the MMT-based materials and NCO– terminated polyurethane prepolymer guaranteed the effective load transfer from TPU matrix to MMT sheets. In Region III, with the progress of the extension, soft segments crystallize and hence a larger stress is required to deform the samples. From Fig. 8(c and d), we can see that the ultimate elongation at break was increased by 46% with the addition of 1.0 wt% MDI-MMT, as compared with that of neat TPU; at the same condition, tensile strength was increased by approximately 70% as compared with that of neat TPU. At low loading (up to 1.0 wt%), MMT layers plasticized the TPU chains by standing between them and increases their free volume; and another important reason for such behavior relied on the existence of multiple H-bonding between the TPU grafted MMT and the adjacent TPU chains.[54] During tensile loading, the motions of TPU chains stimulate the movement of grafted MMT, which was bonded to another MMT *via* another TPU chain. Hence, most of the tensile load was transferred by the H-bonds present between the covalently bonded TPU chains. An additional increase in load leads to disruption of H-bonds and slipping of MMT layers over one another, causing an increase in elongation at break as compared to the neat TPU. At higher loadings, tensile strength and elongation at break decreased due to inhibition of molecular rearrangement and orientation with respect to the tensile axis. A larger value of elongation at break also proved that the nanoscale MMT layers preferentially reinforced the HS of TPU rather than SS.[50] This phenomenon is observed because MDI acted as a bridge to bond MMT sheets and TPU matrix through covalent bonds and the strong interactions between MMT and TPU matrix, in such structures of the TPU/MDI-MMT nanocomposites.

3.4.2. DMA analysis. The thermo-mechanical behavior and reinforcing effect of the exfoliated MMT layers in the TPU/MDI-MMT nanocomposites is assessed by dynamic mechanical analysis (DMA). DMA results were expressed by three main parameters, *i.e.* the storage modulus (E'), the loss modulus (E'') and the damping behavior (tan δ) that is useful for determining the occurrence of molecular mobility transitions such as the glass transition temperature (T_g). DMA analysis is carried out to monitor the temperature dependence of the E', E'' and T_g from tan δ peak values of neat TPU and the TPU/MDI-MMT nanocomposites; results are shown in Fig. 9.

As shown in Fig. 9(A), the significant enhancement of E' for all TPU/MDI-MMT nanocomposites over that of TPU matrix indicated that MMT sheets had strong effect on the elastic properties of TPU due to the restricted movement of TPU chains resulted by the dispersed MDI-MMT. The significant increase in E' is marked above the glass transition region because the relative reinforcing effects of rigid MMT sheets on TPU matrix was enhanced over this temperature change. Results were also supported by the contribution of hydrodynamic reinforcing effect ascribed to the dispersion of the nanosized filler in TPU matrix, which was well controlled by the shape factor and filler volume fraction of the MDI-MMT.[27] A sharp drop in E' after 70 °C confirmed the T_g

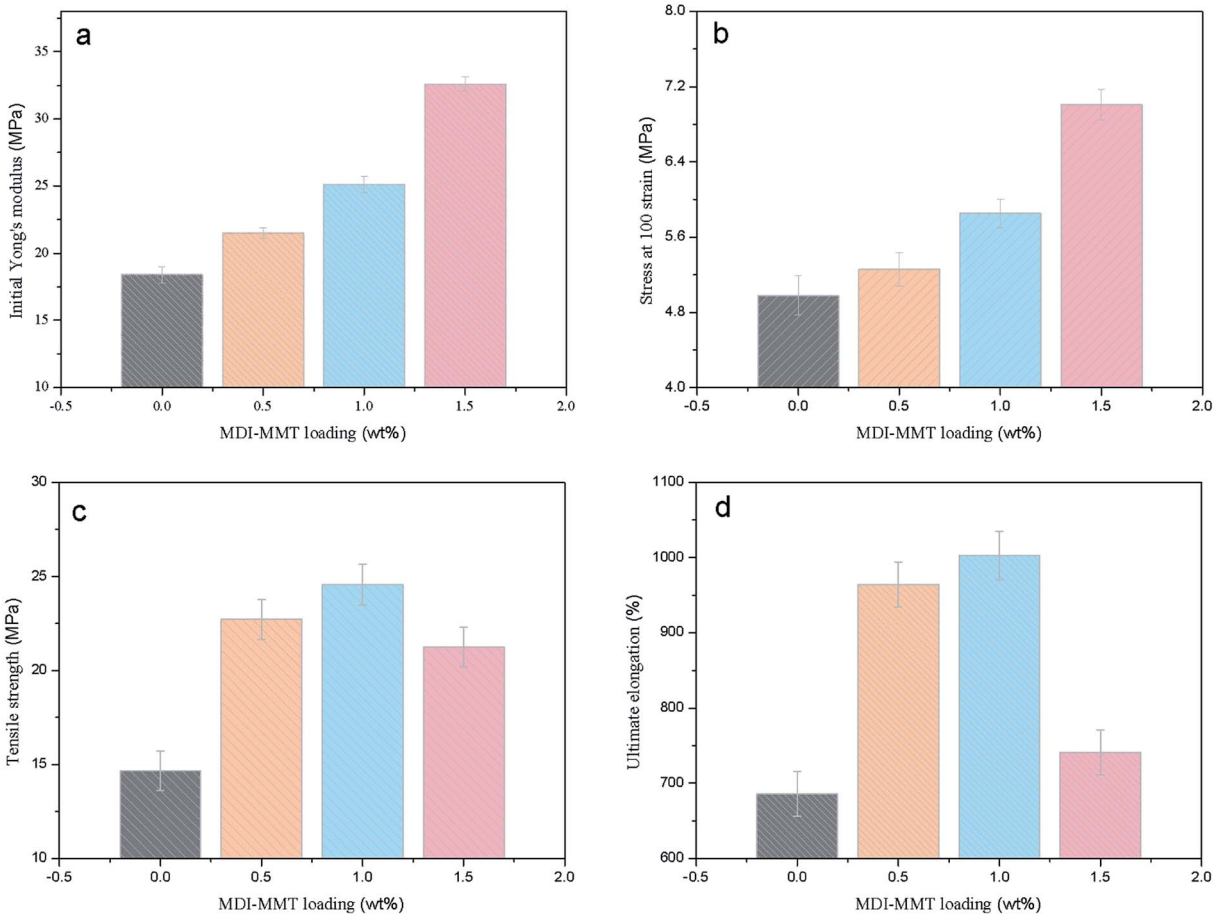

Fig. 8 Tensile mechanical properties of (a) initial Yong's modulus, (b) stress at 100 strain, (c) tensile strength and (d) ultimate elongation at break of neat TPU and TPU/MDI-MMT nanocomposites at different MDI-MMT loadings.

region as modulus decrease drastically from the glassy state to the rubbery state. A drop of modulus has taken place around 1 °C in contrast with the TPU matrix because of the disordering of the PTMG microcrystalline domains of the soft segments. The TPU matrix that is free from MMT showed rapid mobilization of the amorphous soft domains. The tan δ curves are shifted significantly to higher temperatures upon the addition of MDI-MMT, which means that T_g had shifted to higher temperatures because of the restricted molecular motion due to the nanoscale distribution of delaminated MMT layers. Furthermore, it is found that the height of the tan δ decreases and the curve broadens with MDI-MMT loadings in the vicinity of T_g. As tan $\delta = E''/E'$, the low tan δ values for the TPU/MDI-MMT nanocomposites are mainly because of larger changes of the E' in the T_g region than that of the E''.

3.4.3. Rheological analysis. Dynamic frequency sweep test was an important technique for inspecting the network formation and nanoscale morphology of nanocomposites. The dynamic frequency scan is used to measure the linear viscoelastic properties of the samples. At low frequency regions of rheological plots, it reflects the effect of exfoliated MMT sheets on the viscoelastic properties of TPU/MDI-MMT nanocomposites; the dependence of modulus and complex viscosity (η^*) on angular frequency (ω) is studied at low frequencies to detect the effects of exfoliated MMT sheets on their viscoelastic properties. Hence, the logarithmic plots of the storage modulus (G') and η^* *versus* ω obtained from the dynamic frequency sweep tests measured at 200 °C for the neat TPU and its nanocomposites are shown in Fig. 10.

Fig. 10(A) exhibits that the magnitudes of G' of the TPU/MDI-MMT nanocomposites is substantially higher than that of neat TPU over the frequency range and increased with MDI-MMT loadings at low frequencies for all compositions, whereas a higher increase of modulus was observed at high frequencies; this is the result of strong filler–polymer interactions due to MMT–matrix tethering, uniform nanoscale dispersion, and much larger surface area of nanoscale MMT sheets exposed to polymer chains.[16] At low frequency regions, G' modulus value is higher; they narrow down at high frequency regions. This phenomenon was observed because at low frequencies, time is long enough to unravel the entanglements thus result in a full relaxation and a low value of G'; at higher frequencies, there is no time for unraveling the chain entanglement, so the modulus values rose.

Fig. 10(B) shows that the η^* decreases as increase MDI-MMT loadings at all frequencies; the magnitudes of η^* of the TPU/MDI-MMT nanocomposites was substantially higher than that of neat TPU over the frequency range due to the movement of

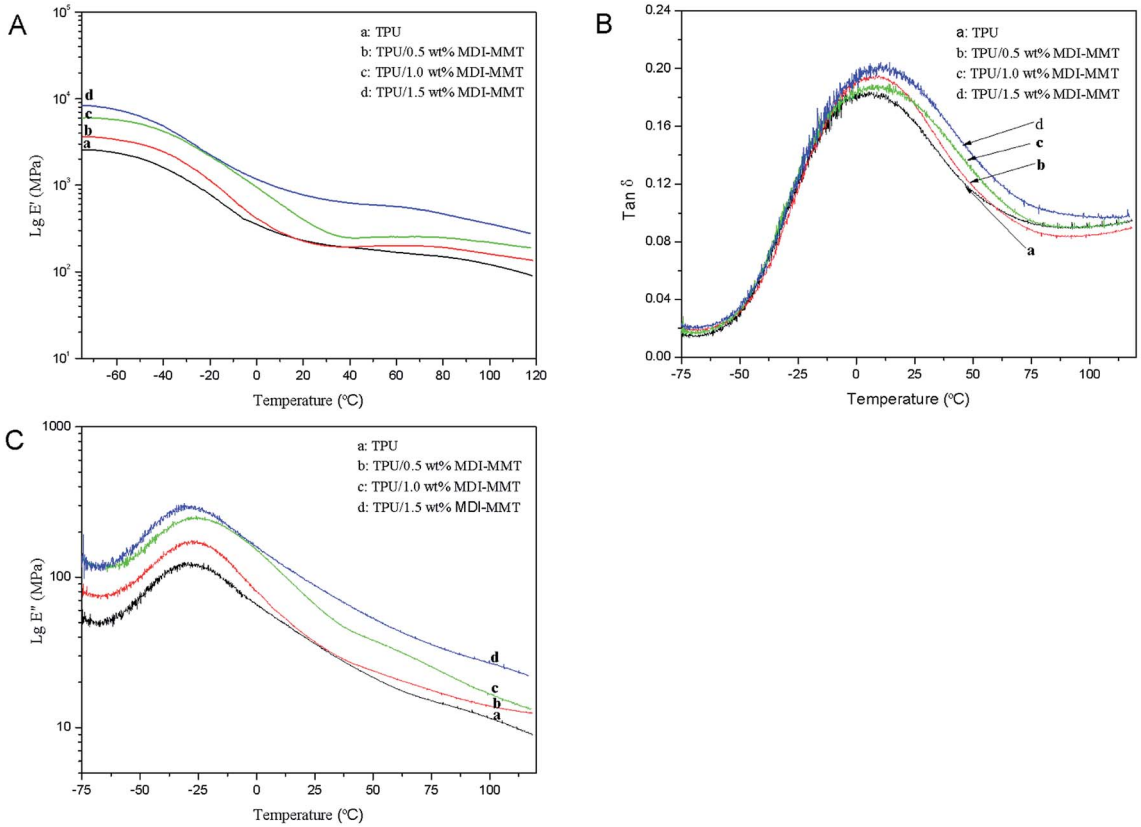

Fig. 9 (A) Typical DMA curves of storage modulus (E'); (B) loss modulus (E''); (C) tan δ of neat TPU and TPU/MDI-MMT nanocomposites at different MDI-MMT loadings, as a function of temperature.

polymer melt result from the exfoliated MMT sheets; the substantial η^* increment of TPU/MDI-MMT nanocomposites as the increase of MDI-MMT loadings should be ascribed to the exfoliated nanoscale MMT sheets' dispersing in TPU matrix. This phenomenon is observed because of the improved compatibility due to the strong interfacial interactions between MDI-MMT sheets and TPU matrix; this enhancement could be explained on the basis of resistance to flow and deformation of the molten polymer chains imposed by tethered nanoscale MMT sheets together with the high aspect ratio, and the shape of the MMT sheets favors the formation of a structural network even at very low MMT contents. The strong shear thinning behavior of TPU/MDI-MMT nanocomposites and their neat equivalent at the melted state is observed due to the increase in the shear stress. The effects on frequency of neat TPU and the TPU/MDI-MMT nanocomposites are depicted in Scheme 3. At low-frequency region, the stress can elongate the soft domain to a maximum extent due to sufficient relax time; however, at high-

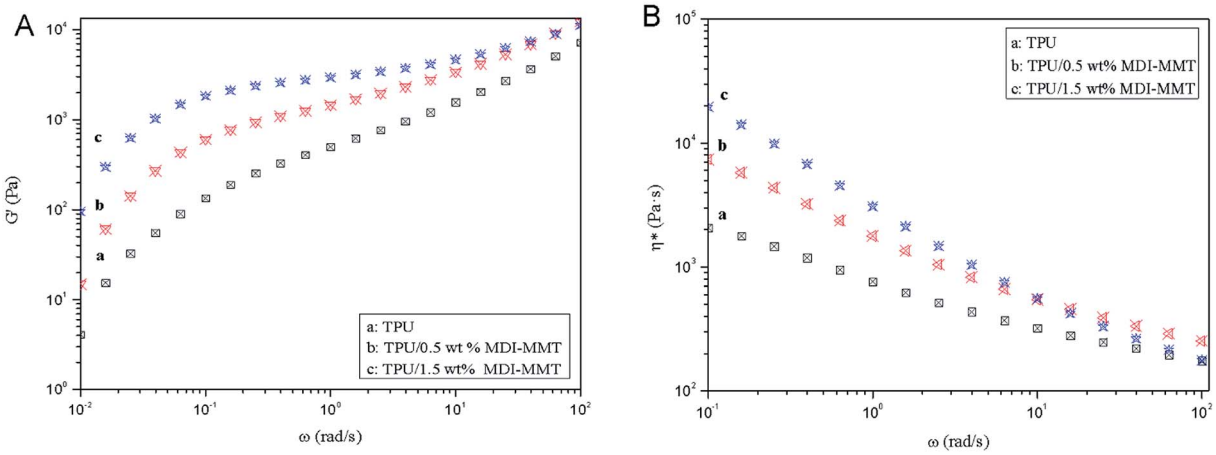

Fig. 10 Typical dynamic frequency sweeps of (A) G', and (B) η^* of neat TPU and TPU/MDI-MMT nanocomposites at different MDI-MMT loadings (at a temperature 200 °C).

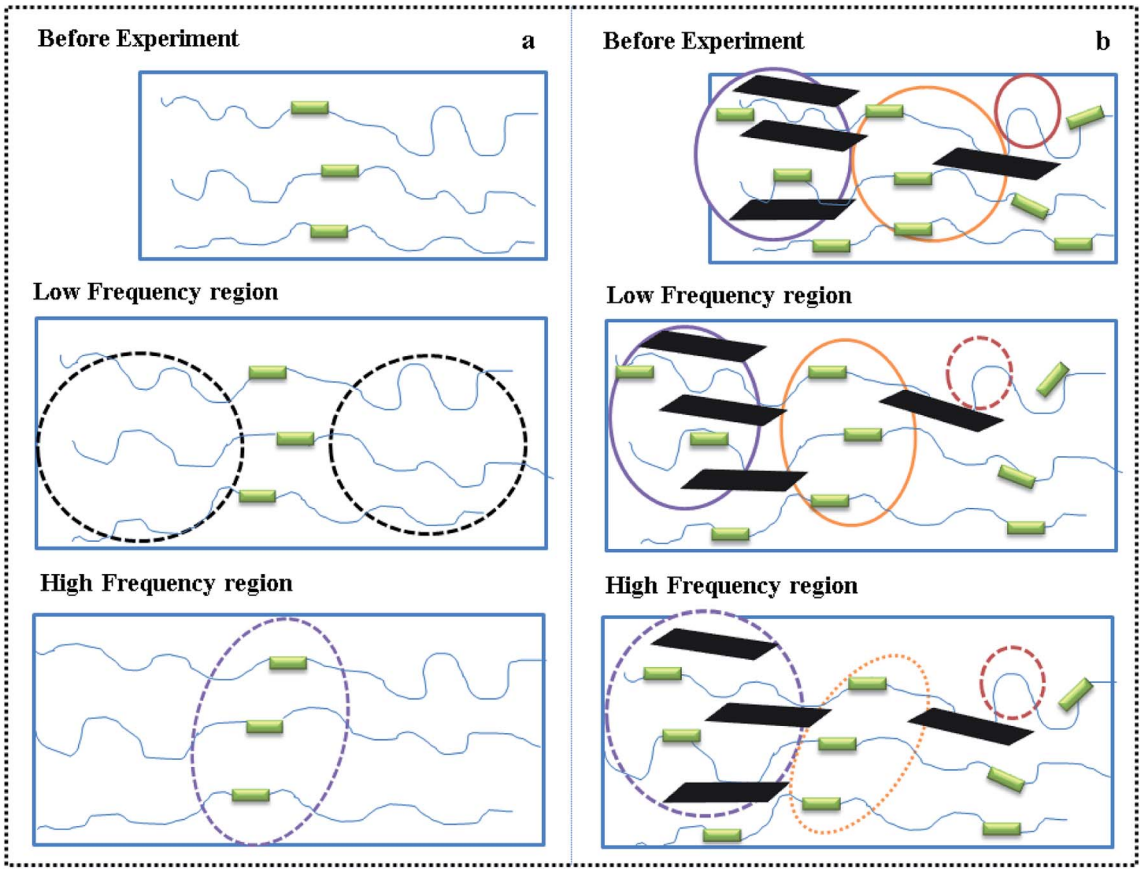

Scheme 3 Effects of frequency on (a) neat TPU and (b) TPU/MDI-MMT nanocomposites.

frequency region, stress gets concentrated mostly on hard domain regions, which is due to unavailability of relax time [Scheme 3(a)]. For the TPU/MDI-MMT nanocomposites, at low-frequency region, the similar result is observed; at high-frequency region, stress gets concentrated mostly on the hard domain region and highly exfoliated MMT sheets aggregates [Scheme 3(b)]. Thus, the shear thinning event occurred at lower MDI-MMT loadings could be explained based on the presence of the exfoliated nanoscale MMT sheets.

4. Conclusions

In summary, we reported a facile method to enhance interfacial interaction between MMT clay and TPU matrix. MDI was grafted on the MMT clay surface, and MDI-MMT sheets were dispersed in the TPU matrix by an *in situ* solution polymerization method. The strong covalent bond between TPU and MDI-MMT clay encourages more ordered packing of the hard segments, promoting polymer phase separation. The stable hard micro-domains in the vicinity of exfoliation MMT sheets hinder the movement of polymer chains, resulting in substantial improvements in mechanical properties, including initial modulus, tensile strength, and elongation at break, at a low clay loading. The presence of strong covalent bonds also increases the stiffness of the TPU at high temperatures, affording the TPU/MDI-MMT nanocomposites for great outdoor applications.

Conflicts of interest

There are no conflicts to declare.

Acknowledgements

This work was financially supported by the Project of Technology Research Center for Lingnan Characteristic Fruits & Vegetables Processing and Application Engineering of Guangdong Province (No. [2015]1487), the Project of Food Science Innovation Team of Guangdong Higher Education Institutes (2016KCXTD020), and Guangdong University of Petrochemical Technology Research Fund (2018rc37), the Projects of Science and Technology of Guangdong (2015B0202300001), and Science and Technology Planning Project of Guangdong Province of China (2016 A040403075).

References

1 S. Pavlidou and C. D. Papaspyrides, *Prog. Polym. Sci.*, 2008, **33**, 1119–1198.
2 Y. C. Chua and X. Lu, *Langmuir*, 2007, **23**, 1701–1710.
3 L. Fogelström, E. Malmström, M. Johansson and A. Hult, *ACS Appl. Mater. Interfaces*, 2010, **2**, 1679–1684.
4 I. Zaman, Q. H. Le, H. C. Kuan, N. K. Kawashima, L. Luong, A. Gerson and J. Ma, *Polymer*, 2011, **52**, 497–504.

5 Y. C. Ke and P. Stroeve, *Polymer-layered silicate and silica nanocomposite*, Elsevier, vol. 6, 2005.
6 N. Hossieny, V. Shaayegan, A. Ameli, M. Saniei and C. B. Park, *Polymer*, 2017, **11**, 208–218.
7 J. Choi, D. S. Moon, J. U. Jang, W. B. Yin, B. Lee and K. J. Lee, *Polymer*, 2017, **3**, 83–90.
8 A. Sut, E. Metzsch-Zilligen, M. Großhauser, R. Pfaendner and B. Schartel, *Polym. Degrad. Stab.*, 2018, **156**, 43–58.
9 L. P. Yang, S. L. Phua, C. L. Toh, L. Y. Zhang, H. Ling, M. C. Chang, D. Zhou, Y. L. Dong and X. H. Lu, *RSC Adv.*, 2013, **3**, 6077–6085.
10 A. K. Barick and D. K. Tripathy, *Polym. Bull.*, 2011, **66**, 1231–1253.
11 S. Benali, G. Gorrasi, L. Bonnaud and P. Dubois, *Compos. Sci. Technol.*, 2014, **90**, 74–81.
12 L. A. Savas, T. K. Deniz, U. Tayfun and M. Dogan, *Polym. Degrad. Stab.*, 2016, **12**, 1–12.
13 M. Joshi, B. Adak and B. S. Butola, *Prog. Mater. Sci.*, 2018, **97**, 230–282.
14 P. Ni, J. Li, J. S. Suo and S. B. Li, *J. Appl. Polym. Sci.*, 2004, **99**, 6–13.
15 W. J. Choi, S. H. Kim, Y. J. Kim and S. C. Kim, *Polymer*, 2004, **45**, 6045–6057.
16 M. Razeghi and G. Pircheraghi, *Polymer*, 2018, **148**, 169–180.
17 A. K. Barick and D. K. Tripathy, *J. Appl. Polym. Sci.*, 2010, **117**, 639–654.
18 J. Pavličević, M. Špírková, M. Jovičić, O. Beraa, R. Poręb and J. Budinski-Simendić, *Composites, Part B*, 2013, **45**, 232–238.
19 M. Špírková, J. Pavličević, A. Strachota, R. Poreba, O. Bera, L. Kaprálková, J. Baldrian, M. Šlouf and N. Lazić, *Eur. Polym. J.*, 2011, **47**, 959–972.
20 E. K. Allcorn, M. Natali and J. H. Koo, *Composites, Part A*, 2013, **45**, 109–118.
21 B. Finnigan, D. Martin, P. Halley, R. Truss and K. Campbell, *Polymer*, 2004, **45**, 2249–2261.
22 K. J. Yao, M. Song, D. J. Hourston and D. Z. Luo, *Polymer*, 2002, **43**, 1017–1020.
23 J. Jordan, K. I. Jacob, R. Tannenbaum, M. A. Sharaf and I. Jasiuk, *Mater. Sci. Eng. A*, 2005, **393**, 1–11.
24 J. Marini, E. Pollet, L. Averous and R. E. S. Bretas, *Polymer*, 2014, **55**, 226–5234.
25 J. P. Mensing, A. Wisitsoraat, D. Phokharatkul, T. Lomas and A. Tuantranont, *Composites, Part B*, 2015, **77**, 93–102.
26 T. Zhou, X. M. Zhou and D. Xing, *Biomaterials*, 2014, **35**, 4185–4194.
27 Q. F. Jing, Q. Liu, L. Li, Z. L. Dong and V. V. Silberschmidt, *Composites, Part B*, 2016, **89**, 1–8.
28 L. Rueda, I. Garcia, T. Palomares, A. Alonso-Varona, I. Mondragon, M. Corcuera and A. Eceiza, *J. Biomed. Mater. Res., Part A*, 2011, **97**, 480–489.
29 M. V. Pergal, I. S. Stefanović, R. Poręba, M. Steinhart, P. M. Jovancic, S. Ostoji and M. Spirkova, *Ind. Eng. Chem. Res.*, 2017, **56**, 4970–4983.
30 B. Finnigan, D. Martin, P. Halley, R. Truss and K. Campbell, *J. Appl. Polym. Sci.*, 2005, **97**, 300–309.
31 A. Pattanayak and S. C. Jana, *Polymer*, 2005, **46**, 3275–3288.
32 S. L. Phua, L. P. Yang, C. L. Toh, G. Q. Ding, S. K. Lau, A. Dasari and X. H. Lu, *ACS Appl. Mater. Interfaces*, 2013, **5**, 1302–1309.
33 Z. Wang and T. J. Pinnavaia, *Chem. Mater.*, 1998, **10**, 3769–3771.
34 S. Miyazaki, T. Karino, H. Endo, K. Haraguchi and M. Shibayama, *Macromolecules*, 2006, **39**, 8112–8224.
35 R. Zolfaghari, A. A. Katbab, J. Nabavizadeh, R. Y. Tabasi and M. H. Nejad, *J. Appl. Polym. Sci.*, 2006, **100**, 2096–2107.
36 J. Xu, Y. Ke, L. Yang, X. Bai, G. L. Zhang, Z. L. Zeng, W. S. Gao and D. M. Gong, *J. Appl. Polym. Sci.*, 2015, **132**, 42626–42637.
37 B. D. Credico, E. Cobani, E. Callone, L. Conzatti, D. Cristofori, M. D'Arienzo, S. Dire, L. Giannini, T. Hanel, R. Scotti, P. Stagnaro, L. Tadiello and F. Morazzoni, *Appl. Clay Sci.*, 2018, **152**, 51–64.
38 N. Salahuddin, S. A. Abo-El-Enein, A. Selim and O. Salah El-Dien, *Appl. Clay Sci.*, 2010, **47**, 242–248.
39 X. Y. Meng, Z. Wang, H. Yu, X. H. Du, S. Y. Li, Y. H. Wang, Z. W. Jiang, Q. Y. Wang and T. Tang, *Polymer*, 2009, **50**, 3997–4006.
40 Z. Dominkovics, J. Hári, E. Fekete and B. Pukánszky, *Polym. Degrad. Stab.*, 2011, **96**, 581–587.
41 L. Yang, S. L. Phua, J. K. Teo, C. L. Toh, S. K. Lau, J. Ma and X. Lu, *ACS Appl. Mater. Interfaces*, 2011, **3**, 3026–3032.
42 M. Qiao, S. Wua, Q. Ran and J. Shen, *Polym. Adv. Technol.*, 2010, **21**, 296–299.
43 Q. J. Ding, B. L. Liu, Q. Zhang, Q. He, B. Hu and J. Shen, *Polym. Int.*, 2006, **55**, 500–504.
44 M. Bera and P. K. Maji, *Polymer*, 2017, **119**, 118–133.
45 A. Marand, J. Dahlin, D. Karlsson, G. Skarping and M. Dalene, *J. Environ. Monit.*, 2004, **6**, 606–614.
46 M. V. Pergal, J. V. Džunuzović, R. Poręba, S. Ostojić, A. Radulović and M. Špírková, *Prog. Org. Coat.*, 2013, **76**, 743–756.
47 (*a*) Y. Y. Zhang, Y. Z. Zhang, Y. Liu, X. L. Wang and B. Yang, *Appl. Surf. Sci.*, 2016, **382**, 144–154; (*b*) Y. Y. Luo, Q. Xiao and B. Y. Li, *RSC Adv.*, 2017, **7**, 34939–34944.
48 K. K. Sadasivuni, D. Ponnamma, B. Kumar, M. Strankowski, R. Cardinaels, P. Moldenaers, S. Thomas and Y. Grohens, *Compos. Sci. Technol.*, 2014, **104**, 18–25.
49 G. G. Chen, Y. M. Ma and Z. N. Qi, *J. Appl. Polym. Sci.*, 2000, **77**, 2201–2205.
50 J. Xu, Y. Ke, Q. Zhou, X. L. Hu, Z. J. Tan, L. Y. Yang, Y. Z. Song, Y. Y. Zhao and G. L. Zhang, *Polym. Compos.*, 2014, **35**, 1210–1221.
51 A. K. Barick and D. K. Tripathy, *Mater. Sci. Eng., A*, 2010, **527**, 812–823.
52 F. Yeh, B. S. Hsiao, B. B. Sauer, S. Michel and H. W. Siesler, *Macromolecules*, 2003, **36**, 1940–1954.
53 S. Thakur and N. Karak, *New J. Chem.*, 2015, **39**, 2146–2154.
54 P. Pokharel and S. Choi, *Composites, Part A*, 2015, **69**, 168–177.

